INORGANIC CHEMISTRY
FRONTIERS

RESEARCH ARTICLE

View Article Online
View Journal | View Issue

Cite this: *Inorg. Chem. Front.*, 2017, **4**, 1200

Stoichiometry of lanthanide(III) complexes with tripodal aminophosphonic ligands – a new solution to an old problem†

Rafał Janicki,*[a] Joanna Gałęzowska*[b] and Anna Mondry[a]

Received 10th April 2017,
Accepted 12th May 2017

DOI: 10.1039/c7qi00191f

rsc.li/frontiers-inorganic

The Eu^{3+} and Gd^{3+} complexes with an *N*-(methylene-2-pyridine)-*N*,*N*-di(methylenephosphonate) ligand (H_4NP_2py), an analogue of nitrilotri(methylphosphonic) acid (H_6NTP), were synthesized and structurally characterized by X-ray single crystal diffraction. The determined crystal structures ($[C(NH_2)_3]_5[Ln(NP_2py)_2]\cdot 12H_2O$) are the first example of a monomeric Ln^{3+} complex encapsulated by two tripodal aminophosphonic ligands. Each of the NP_2py anions coordinates to Ln^{3+} through two oxygen atoms from each monodentate phosphonic group, amine nitrogen and pyridine nitrogen atoms, filling thus 8 coordination sites of Ln^{3+}. The luminescence properties of $[C(NH_2)_3]_5[Eu(NP_2py)_2]\cdot 12H_2O$ crystals were studied and compared with those of Eu–NP_2py complexes in solution. Speciation analysis of Ln–NP_2py complexes (Ln : NP_2py = 1 : 2), performed by luminescence and potentiometric methods, showed that both $[Ln(NP_2py)]^-$ and $[Ln(NP_2py)_2]^{5-}$ species may exist in solution. However, the formation of the latter one occurs in alkaline solutions at pH as high as 8. By implementing the Specific Ion Interaction Theory (SIT) it was possible to calculate the thermodynamic stability constants of the $[Eu(NP_2py)]^-$ and $[Eu(NP_2py)_2]^{5-}$ complexes. The corresponding $\log \beta^0_{EuL}$ and $\log \beta^0_{EuL2}$ values are 16.3 ± 0.11 and 19.5 ± 0.15, respectively.

Introduction

The chemistry of metal-phosphonates has attracted increasing attention over the last few decades due to the variety of properties that can be introduced *via* a phosphonic moiety.[1] (Poly) aminopolyphosphonates are very strong complexing agents for alkaline earth, transition and rare earth metal ions.[2] Owing to the high basicity of the oxygen atoms,[3,4] phosphonates interact with cations more strongly than their carboxylic analogues and are able to create more stable complexes.[5,6] Phosphonate complexes with luminescent, paramagnetic lanthanide ions[7,8] play a significant role as promising phosphors for new technologies and potential contrast agents in magnetic resonance imaging (MRI)[9] as well as paramagnetic shift reagents for biologically important cations (*e.g.* Na^+).[10] Owing to its good pharmacokinetics, biodistribution and bone-seeking properties the ^{153}Sm-EDTP complex,[1a,6e–h] known as QUADRAMET®, was approved by the US FDA for use of painful skeletal metastases in humans.[1d,11]

In general, polyaminopolyphosphonic acids are the analogues of the nitrilotris(methylenephosphonic) acid (hereinafter referred to as NTP). To date the NTP ligand has found many applications[12] driven in many cases by coordination properties of this ligand in Ln^{3+} complexes.[13] Because the majority of its applications are related to the NTP properties in aqueous solution, it seems particularly important to study its properties in this medium. However, the formation of the Ln^{3+} complexes with ligands of the NTP type in solution remains still not fully understood. For example it is unclear whether bis(nitrilotris(methylenephosphonato))lanthanide complexes are

[a]*Faculty of Chemistry, University of Wrocław, F. Joliot-Curie 14, 50-383 Wrocław, Poland. E-mail: rafal.janicki@chem.uni.wroc.pl*
[b]*Department of Inorganic Chemistry, Wrocław Medical University, Borowska 211A, 50-556 Wrocław, Poland. E-mail: joanna.galezowska@umed.wroc.pl*

†Electronic supplementary information (ESI) available: Table 1S. The fitting parameters for eqn (3), determined from the spectra of the $^5D_0 \rightarrow {}^7F_{1,2,4}$ transitions of the $[Eu(NP_2py)_2]^{5-}$ complex in aqueous solution; Table 2S. Selected luminescent data of Eu–NP_2py and Tb–NP_2py systems; Table 3.The complex formation constants of NP_2Py with Sm^{3+}, Eu^{3+}, Gd^{3+} and Tb^{3+} at 25 °C, I = 0.1 mol dm^{-3} ($NaClO_4$), in 1 : 1 and 1 : 2 molar ratios Ln : L; Table 4S. Stability constants of NP_2Py with Eu^{3+} at 25 °C in different ionic strengths (KCl); Fig. 1S. Phosphorescence spectrum of $[C(NH_2)_3]_5[Gd(NP_2py)_2]\cdot 12H_2O$ crystals at 77 K; Fig. 2S. The plot of luminescence quantum yields of Tb : NP_2py 1 : 1 and 1 : 2 systems *versus* pH; Fig. 3S. UV spectra of the NP_2py ligand and Tb : NP_2py complex at various pH; Fig. 4S. Plot of q_{H2O} *versus* pH of solution for the Eu–NP_2py complex with Eu : NP_2py ratios of 1 : 1 and 1 : 2. The Δq_{H2O} is the difference between q_{H2O} for 1 : 1 and 1 : 2 solutions at the same pH; Fig. 5S. Plot of q_{H2O} *versus* pH of solution for the Tb–NP_2py complex with Tb : NP_2py ratios of 1 : 1 and 1 : 2; Fig. 6S. Species distribution curves of H_6NP_2py acid (L). Charges omitted for brevity; Fig. 7S. Species distribution curves for the Ln^{3+}–N_2Py complexes as a function of pH for a 1 : 1 Ln : L molar ratio (A) and 1 : 2 Ln : L (B). Equimolar complexes are marked in blue, biscomplexes in red color, I = 0.1 M $NaClO_4$, 25 °C. CCDC 1541894 and 1541895. For ESI and crystallographic data in CIF or other electronic format see DOI: 10.1039/c7qi00191f

formed in solution at all.[14–16] Moreover no crystal structures of monomeric Ln^{3+} complexes with tripodal aminophosphonic ligands have been reported so far. The high negative charge of the NTP ligand (−6) and the presence of rather bulky phosphonic groups are probably the main factors destabilizing the $[Ln(NTP)_2]^{9-}$ complexes in solution.

The aim of this paper is to study the chemical properties of a modified NTP ligand – *N*-(methylene-2-pyridine)-*N*,*N*-di(methylenephosphonic) acid (hereinafter referred to as NP_2py – Scheme 1) to establish finally whether, $[Ln(NP_2py)_2]^{5-}$ complexes may be indeed formed in solution.[17]

We have focused our attention on the stoichiometry and stability of species in the solution of the Ln–NP_2py system by implementing various physical methods such as X-ray crystallography, luminescence spectroscopy, potentiometry as well as a theoretical approach based on Specific Ion Interaction Theory (SIT).[18] Because coordination of aminopolyphosphonates to Ln^{3+} cations has not been completely clear, we believe that the presented data may be helpful in understanding the interaction of this important class of ligands with lanthanide ions in solution, in general.

Results and discussion

Crystal structures

The crystal structures of compounds of the following formula $[C(NH_2)_3]_5[Ln(NP_2py)_2]\cdot 12H_2O$ (Ln = Eu or Gd) were determined. The crystals of both compounds are isostructural and belong to the $P\bar{1}$ space group. The asymmetric unit comprises one $[Ln(NP_2py)_2]^{5-}$ complex anion, five guanidinium cations out of which one is disordered and twelve water molecules out of which two are disordered. The monomeric $[Ln(NP_2py)_2]^{5-}$ complex anions are completely deprotonated and their negative charge is compensated by $[C(NH_2)_3]^+$ cations.

Two anionic $[NP_2py]^{4-}$ ligands are bound to the Ln^{3+} cation. Each of them is linked with the Ln^{3+} by two oxygen atoms from both monodentate phosphonic groups, one tertiary nitrogen atom and one pyridine nitrogen atom, filling thus four coordination sites of the Ln^{3+} cation. The molecular structure of the $[Eu(NP_2py)_2]^{5-}$ complex is presented in Fig. 1. The selected Ln–L bond lengths are presented in Table 1.

As is seen the Eu–L and Gd–L bond lengths are similar within the error of bond length estimation. The Ln–L bond lengths increase in the order Ln–O < Ln–$N_{(py)}$ < Ln–$N_{(am)}$ which reflects the sequence of ligand donor properties.[19]

The coordination polyhedron of the Ln^{3+} cation may be described as a distorted prism (Fig. 2). The Ln^{3+} cation lies in the general position, but the approximate symmetry of the complex anion is C_i, as shown in Fig. 2.

The $[Ln(NP_2py)_2]^{5-}$ complexes are held together by a network of hydrogen bonds and electrostatic interactions. Owing to the high negative charge of the anionic $[Ln(NP_2py)_2]^{5-}$ complex the distance between the neighbouring anions is large and the anionic complexes are well separated from each other; the shortest Eu·····Eu' and Gd·····Gd' distances are 10.47(7) Å and 10.37(7), respectively.

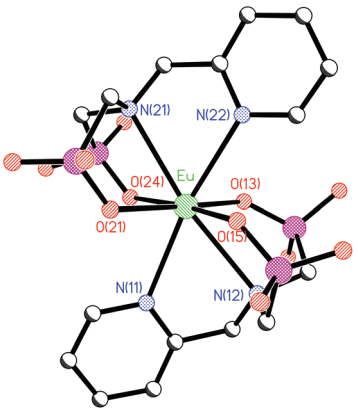

Fig. 1 Molecular structure of the $[Eu(NP_2py)_2]^{5-}$ complex; the H atoms are omitted for clarity.

Table 1 Selected Ln–L bond lengths in Å

Bond lengths	Eu	Gd
Ln–O21	2.315(2)	2.308(5)
Ln–O13	2.337(2)	2.328(5)
Ln–O15	2.319(2)	2.316(5)
Ln–O24	2.353(2)	2.347(5)
Ln–$O_{(aver.)}$	**2.331(18)**	**2.325(17)**
Ln–$N12_{(am)}$	2.770(3)	2.764(7)
Ln–$N21_{(am)}$	2.751(3)	2.744(7)
Ln–$N_{(am\ aver.)}$	**2.761(13)**	**2.754(14)**
Ln–$N11_{(py)}$	2.596(3)	2.592(7)
Ln–$N22_{(py)}$	2.657(3)	2.634(6)
Ln–$N_{(py\ aver.)}$	**2.626(43)**	**2.613(29)**

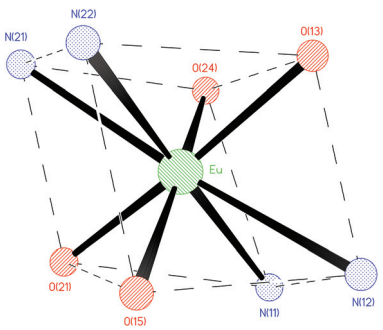

Fig. 2 The coordination polyhedra of Eu^{3+} in the $[Eu(NP_2py)_2]^{5-}$ complex anion.

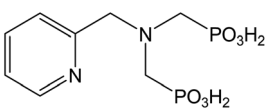

Scheme 1 Chemical structure of *N*-(methylene-2-pyridine)-*N*,*N*-di(methylenephosphonis acid) – H_4NP_2py.

Luminescence spectra of the $[C(NH_2)_3]_5[Eu(NP_2py)_2]\cdot 12H_2O$ crystal

Out of Ln^{3+} the Eu^{3+} f–f transitions are characterized by a simple and informative spectral pattern that is why we have chosen this cation for detailed spectroscopic studies.

The luminescence spectra of the $[C(NH_2)_3]_5[Eu(NP_2py)_2]\cdot 12H_2O$ crystal were observed when the Eu^{3+} was excited into f–f transitions as well as into ligand states. The luminescence excitation spectrum of the crystals under study is presented in Fig. 3.

Narrow peaks attributed to the f–f transitions of the Eu^{3+} and broad band of the ligand ($^1\pi \rightarrow {}^1\pi^*$, $^1n \rightarrow {}^1\pi^*$) are observed in the spectrum. The presence of the latter band indicates that the energy transfer from the ligand to the Eu^{3+} states occurs. The luminescence spectrum of the $[C(NH_2)_3]_5[Gd(NP_2py)_2]\cdot 12H_2O$ complex indicates that the position of the triplet state of the ligand is centered at ~437 nm, Fig. 1S.† [20] The luminescence spectrum of the $[C(NH_2)_3]_5[Eu(NP_2py)_2]\cdot 12H_2O$ crystal excited into the ligand band is shown in Fig. 4. The emission intensities of the $^5D_0 \rightarrow {}^7F_J$ transitions in relation to the $^5D_0 \rightarrow {}^7F_1$ one are also included in this figure.

Five bands attributed to the electronic transitions from the excited $^5D_0$ to the lower lying $^7F_{0,1,2,3,4}$ states are observed in the spectrum. All these transitions are induced electric dipole (ED) transitions, except for the $^5D_0 \rightarrow {}^7F_1$, which is of magnetic dipole (MD) character. Thus the $^5D_0 \rightarrow {}^7F_1$ transition may be used as a reference since its intensity does not depend on the chemical surrounding of Eu^{3+}.[21] The $^5D_0 \rightarrow {}^7F_0$ and $^5D_0 \rightarrow {}^7F_3$ transitions are forbidden due to the selection rules. For this reason, the intensities of these transitions are usually very low as compared with those of $^5D_0 \rightarrow {}^7F_{1,2,4}$ transitions. Since the ground $^7F_0$ and the emitting $^5D_0$ states are nondegenerate, the $^5D_0 \leftrightarrow {}^7F_0$ transitions consist of a single unsplit line for the given Eu^{3+} surrounding. Therefore there is a one to one correspondence between the number of lines in the spectrum of this transition and the number of chemically distinct environments of the Eu^{3+} ion. The energy levels of the $^7F_{1,2,3,4}$ multiplets and their crystal field (e) as well as vibronic (v) components found in the RT spectra are presented in Table 2.

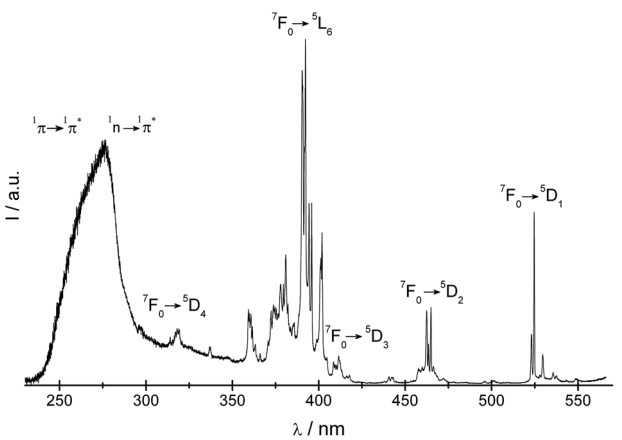

Fig. 3 Luminescence excitation spectrum (λ_{em} = 592.35 nm) of the $[C(NH_2)_3]_5[Eu(NP_2py)_2]\cdot 12H_2O$ crystals.

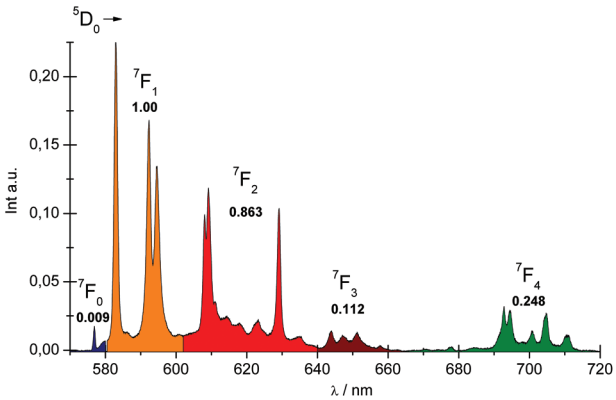

Fig. 4 Luminescence spectrum of the crystal under study (λ_{ex} = 276 nm).

Because $^5D_0 \rightarrow {}^7F_{0,2,3,4}$ transitions are strictly forbidden in centrosymmetric systems, the presence of these transitions in the luminescence spectrum indicates that the C_i symmetry of the $[Eu(NP_2py)_2]^{5-}$ complex in the crystal is approximate. The determined luminescence lifetime of the $^5D_0$ state at RT is 1840 μs.

The next step of our studies was the analysis of the spectroscopic properties of the Eu–NP_2py complex in aqueous solution.

Luminescence spectra of the Eu–NP_2py and Tb–NP_2py systems in solution

Ln–NP_2py complexes with the metal to ligand ratio 1 : 1. Taking into account Eu–L bond lengths it may be reasonably assumed that the encapsulation of the Ln^{3+} cation by the NP_2py ligand is achieved by the coordination of phosphonic and pyridine groups. The binding of the N(imino) atom to the

Table 2 The energy of the crystal field and vibronic lines of the selected multiplets for the $4f^6$ configuration at RT. Δ_{CFS} is the energy difference between the highest and lowest CF components of the $^{2S+1}L_J$ multiplet

$^{2S+1}L_J$	E/cm^{-1}		$^{2S+1}L_J$	E/cm^{-1}	
$^7F_1$	180	e	$^7F_3$	1800	e
	452	e		1880	e
	512	e		1979	v
Δ_{CFS}	332			2131	e
			Δ_{CFS}	331	
$^7F_2$	889	e	$^7F_4$	2577	e
	919	e		2717	v
	967	v		2901	e
	1050	v		2935	e
	1145	v		3007	v
	1259	v		3064	e
	1287	v		3144	e
	1440	e		3256	e
	1585	v		3269	e
Δ_{CFS}	550		Δ_{CFS}	692	

Ln^{3+} is forced by the former ones. In this context, it seems to be important to indicate how the coordination of phosphonate and pyridine groups depends on the pH of a solution. In order to find the binding mode of the NP_2py ligand and the stoichiometry of the formed Ln–NP_2py species, the luminescence spectra of Eu–NP_2py and Tb–NP_2py complexes in aqueous solution were recorded. The selected luminescence spectra of the Eu–NP_2py complex at different pH are presented in Fig. 5.

At pH 2.26 the intensity of the hypersensitive $^5D_0 \rightarrow {}^7F_2$ transition (1.08) is similar to that of the magnetic dipole $^5D_0 \rightarrow {}^7F_1$ transition and higher than the relative intensity for the aqua ion (0.68). The increase of pH brings about an increase of the relative intensity of the $^5D_0 \rightarrow {}^7F_2$ transition from 1.08 (pH = 2.26) to 2.74 (pH = 10.5). It means that the NP_2py ligand starts to coordinate at pH ~2.26. Under these conditions competing reactions undergo between the protonation and coordination of phosphonate groups to the Eu^{3+}.

The protonation of the N_{py} atom at low pH prevents the Eu–N_{py} interaction and consequently may hinder the L–Eu energy transfer. Therefore the question arises whether the efficiency of an antenna effect as a function of pH may serve as a coordination probe for establishing the binding of pyridine to the Eu^{3+}. In general the Tb^{3+} compounds are more convenient to study the energy transfer process in comparison with those of Eu^{3+} for which the ligand band may be imposed on the L–M charge transfer spectra of Eu^{3+}.[22] Accordingly, to find the pH range in which the coordination of the pyridyl group to the Ln^{3+} occurs, the luminescence spectra of the Tb–NP_2py complex at various pH with an excitation wavelength of 266 nm were recorded (Fig. 6). The oscillator strengths of the $^1\pi \rightarrow {}^1\pi^*$, $^1n \rightarrow {}^1\pi^*$ transition calculated from absorption spectra *versus* pH are also presented in the insert of this figure.

As can be seen the largest increase of the luminescence intensity of all f–f transitions is observed between pH 3 and 5.5. Simultaneously the oscillator strength of the ligand band monotonically decreases. These results indicate that the changes of the efficiency of the antenna effect may be used to study the coordination modes of chromophore groups to the Tb^{3+}. The determined values of luminescence quantum yields

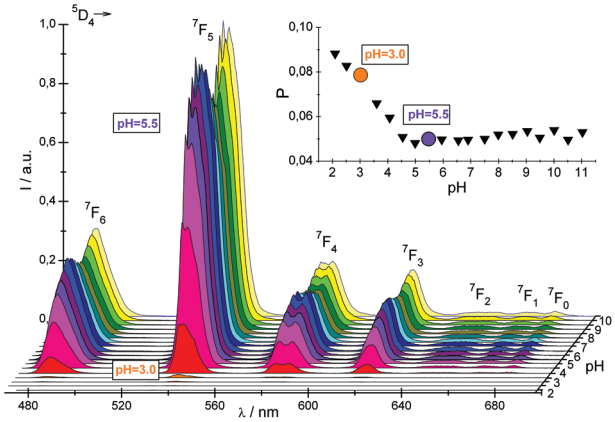

Fig. 6 Luminescence spectra of the Tb–NP_2py 1 : 1 complex at different pH. The plot of the oscillator strengths of the $^1\pi \rightarrow {}^1\pi^*$, $^1n \rightarrow {}^1\pi^*$ transition *versus* pH is shown in the insert.

Φ_{Tb3+} of the Tb : NP_2py 1 : 1 and 1 : 2 systems (Fig. 2S†) may confirm this conclusion.

It is also worth considering the changes of the energy of the ligand centered transitions, caused by coordination of the NP_2py ligand to the Tb^{3+} (Fig. 3S†). Because the $^1\pi \rightarrow {}^1\pi^*$, $^1n \rightarrow {}^1\pi^*$ transitions are particularly sensitive to the interaction of the N pyridine atom with the metal cation, a remarkable bathochromic shift of the ligand band (~550 cm^{-1}) is observed in the spectra of the Tb–NP_2py complex at pH above 6 as compared with the spectra of the free ligand (see Fig. 3S). The observed changes of the f–f and ligand bands above pH ~ 3 support the conclusion that the coordination of the pyridyl group to the Tb^{3+} occurs at pH between 3.0 and 5.5. The coordination of the NP_2py ligand is completed above pH = 6.

Ln–NP_2py complexes with the metal to ligand ratio 1 : 2. The luminescence spectra of the Eu–NP_2py system with the Eu : L = 1 : 2 in solutions at different pH are presented in Fig. 7.

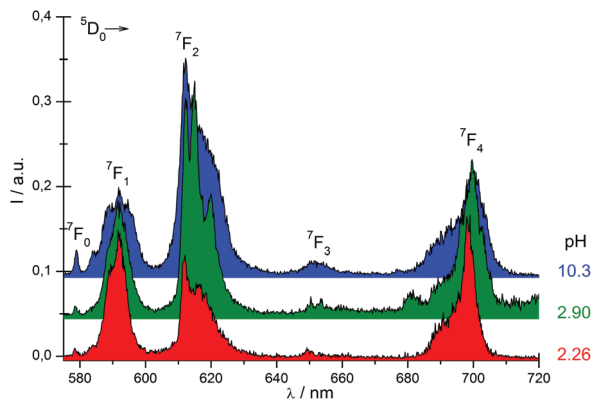

Fig. 5 Luminescence spectra of the Eu–NP_2py complex (λ_{ex} = 393 nm, Eu : NP_2py = 1 : 1) in aqueous solution at different pH.

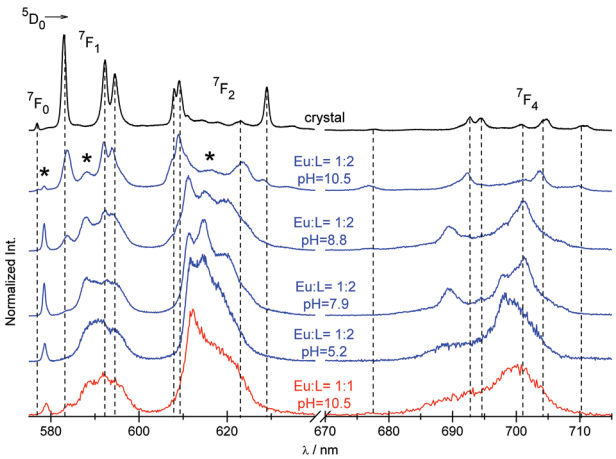

Fig. 7 Luminescence spectra of the crystal and solutions of Eu^{3+} : NP_2py = 1 : 2 and 1 : 1. The bands attributed to the $[Eu(NP_2py)]^-$ species are marked with asterisks.

As can be seen in Fig. 7 the spectral pattern of f–f bands strongly depends on pH. A qualitative comparison between the spectra of the crystal and solutions of the Eu : NP_2py = 1 : 2 complex demonstrates that at pH = 10.5 $[Eu(NP_2py)_2]^{5-}$ is a predominant species. As the pH decreases, the CF components of individual multiplets of the $[Eu(NP_2py)_2]^{5-}$ complex vanish and below pH 8 they completely disappear. It may suggest that the formation of the $[Eu(NP_2py)_2]^{5-}$ complex starts at pH ~ 8. The presence of additional bands (marked with an asterisk in the spectra in Fig. 7) may indicate that the other species, different to that found in the crystal, also exist in solution.

Owing to the simplicity of the $^5D_0 \rightarrow {}^7F_0$ spectrum it was used to monitor the changes in the nearest coordination sphere of the Eu^{3+} cation. The luminescence spectra of the $^5D_0 \rightarrow {}^7F_0$ transition of solutions and the crystal are presented in Fig. 8.

Two well separated $^5D_0 \rightarrow {}^7F_0$ peaks in the spectrum of the solution of the Eu : NP_2py = 1 : 2 system at pH 10.5 are observed. The comparison of the energy of these peaks with those in the crystal and the solution of Eu : NP_2py = 1 : 1 at pH = 10.5 enabled us to attribute the higher energy peak at 17 330 cm^{-1} to the $[Eu(NP_2py)_2]^{5-}$ species, while the lower energy peak centered at 17 286 cm^{-1} to the $[Eu(NP_2py)]^{-}$ species. Both $^5D_0 \rightarrow {}^7F_0$ peaks are separated by 56 cm^{-1}. This difference is probably caused by the change of the number of donor atoms and/or number of water molecules coordinated to the Eu^{3+} (see section "Number of coordinated H_2O molecules to the Eu^{3+} cation" in the ESI†).

Quantitative analysis of the EuL + L ⇆ EuL_2 reaction. In the next step we focused our attention on a quantitative description of the reaction (1) expressed by the equilibrium constant K_{12}

$$[Eu(NP_2py)]^{-} + NP_2py^{4-} \leftrightarrows [Eu(NP_2py)_2]^{5-} \quad (1)$$

$$K_{12} = \frac{[Eu(NP_2py)_2^{5-}]}{[Eu(NP_2py)^{-}]\cdot[NP_2py^{4-}]} \quad (2)$$

To determine the K_{12} constant we used the method based on the fitting of the spectra of the crystals to those of solutions.[23] The spectrum of the crystal under study served us as a model of 1 : 2 species while the spectrum of Eu–NP_2py 1 : 1 at pH = 10.5 was used as the spectrum of a pure 1 : 1 complex. However owing to the dynamic effects,[23,24] the spectra of f–f transitions in the solution are broadened in comparison to the spectra of the crystal. For this reason the simulated spectra of the $[Eu(NP_2py)_2]^{5-}$ species derived from the spectra of the crystal were artificially broadened. The equation that was used to calculate the simulated spectrum of the $[Eu(NP_2py)_2]^{5-}$ species in solution is as follows:

$$J_{calc} = \left(\sum_{i=1}^{z} A_{12} J_{max} \frac{\exp\left[-0.3 \cdot \frac{\lambda - \lambda_{max}}{B_{12} \cdot \Delta\lambda}\right]}{\left[1 + \left(\frac{\lambda - \lambda_{max}}{B_{12} \cdot \Delta\lambda}\right)^2\right]} \right) \quad (3)$$

where:

J_{calc} – intensity at a given value of λ;

z – the number of peaks for the given $^5D_0 \rightarrow {}^7F_J$ transition;

J_{max} – the maximum intensity of the peak;

λ_{max} – the wavelength of the peak maximum;

$\Delta\lambda$ – the half-width of a peak;

A_{12} and B_{12} are adjustable parameters connected with artificial broadening of bands.

The final set of parameters used to calculate the simulated spectrum of the $[Eu(NP_2py)_2]^{5-}$ species is presented in Table 1S (ESI†). The simulated and experimental spectra of compounds under study are shown in Fig. 9.

Next, the simulated spectra of the $^5D_0 \rightarrow {}^7F_{1,2,4}$ transitions were used to calculate the molar fractions χ of $[Eu(NP_2py)]^{-}$ and $[Eu(NP_2py)_2]^{5-}$ species (Table 3).

The average molar fractions of $[Eu(NP_2py)_2]^{5-}$and $[Eu(NP_2py)]^{-}$ species are ~81% and ~19%, respectively. These results are consistent, within the error of experimental limits (±10%), regardless of the transition taken for the calculation.

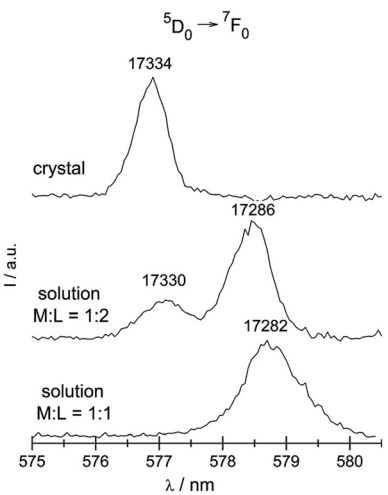

Fig. 8 Luminescence spectra of the $^5D_0 \rightarrow {}^7F_0$ transition of the Eu–NP_2py complexes in the crystal and in solutions at pH = 10.5.

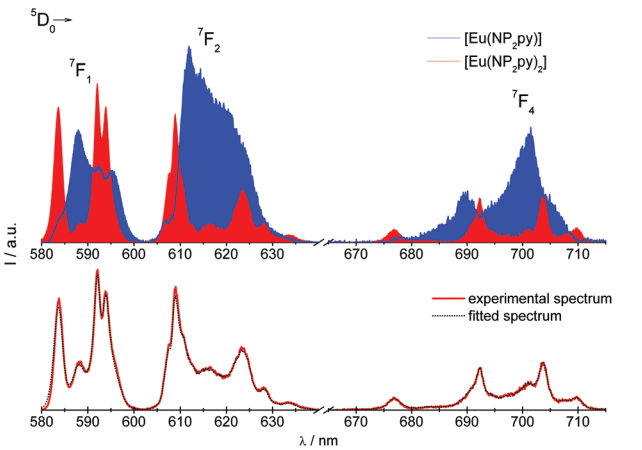

Fig. 9 Simulated spectra of the $[Eu(NP_2py)_2]^{5-}$ (red) and $[Eu(NP_2py)]^{-}$ (blue) species. The fitted and experimental spectra of the Eu : NP_2py 1 : 2 system at pH 10.5.

Table 3 Molar fractions χ of $[Eu(NP_2py)]^-$ and $[Eu(NP_2py)_2]^{5-}$ species in aqueous solution at pH = 10.5 determined from various $^5D_0 \rightarrow {}^7F_{1,2,4}$ transitions

Transition	χ [Eu(NP$_2$py)]–	χ [Eu(NP$_2$py)$_2$]$^{5-}$	log K_{12}
$^5D_0 \rightarrow {}^7F_1$	25% ± 10%	75% ± 10%	4.2 ± 0.5
$^5D_0 \rightarrow {}^7F_2$	18% ± 10%	82% ± 10%	4.5 ± 0.5
$^5D_0 \rightarrow {}^7F_4$	15% ± 10%	85% ± 10%	4.6 ± 0.5
Average	19(5)	81(5)	4.4 ± 0.5

The estimated averaged value of log K_{1-2} for the reaction (1) is about 4.4 ± 0.5.

It should be noted that the presented speciation analysis for the case of f-elements is not always feasible, because the complexes existing in equilibrium are usually characterized by similar spectral patterns as it was shown previously by Horrocks *et al.* for the case of lanthanide complexes with NTP.[15]

To support the presented results the analysis was extended by potentiometric measurements.

Potentiometric study

Protonation of the ligand. We performed potentiometric titrations of a free ligand in order to determine its acid–base properties. The fully protonated form of the H_4NP_2py possesses six dissociable protons $[H_6L]^{2+}$ (see Fig. 6S†) two at each phosphonic group, one at the pyridine moiety and one on the central tertiary N amine atom. However, it was possible to determine only four protonation constants (K_1–K_4) because the K_5 and K_6 values corresponding to the dissociation of one proton from each of the PO_3H_2 groups can be determined only for solutions at pH below 2. This is beyond the available range for standard potentiometric titrations, and the log K_5 and log K_6 values were determined previously by the NMR method.[17] Measurements in different ionic strengths (KCl): 0.075 M, 0.1 M, 0.2 M, 0.5 M, 1 M and 2 M were also performed. The calculated log K_n values are listed in Table 4.

The most basic constant log K_1 = 10.63(2) (Table 4) corresponds to the protonation of the nitrogen of the tertiary amino group and is two logarithmic units higher than that of H_6NTP acid.[14,25–27] The values of this constant for NTP, determined by potentiometric methods in 0.1 M ionic strengths in different electrolytes at 25 °C were found to be: 12.7(1),[14] 12.8(2),[25] 12.20(6),[26] 12.5.[27] Such a decrease of the highest protonation constant of H_4NP_2py is clearly caused by substitution of one of the phosphonic groups by the pyridine moiety. The same phenomenon has been noticed by Kurzak *et al.*[28] in *N*-3-picolyliminodi(methylenephosphonic) acid (NP_3py); the log K value of the tertiary amine was found to be 10.40(1) in 0.2 M KCl. The following deprotonation steps of H_4NP_2py release the protons from both phosphonic groups; log K_2 = 6.74(4), log K_4 = 2.23(5) and the pyridine moiety; log K_3 = 5.61(4) (Table 4). Such deprotonation of H_4NP_2py is consistent with ^{31}P NMR results[17] and based on those data it was concluded that the third and fourth dissociation steps occur at pH between 2 and 3 (log K_4) and 4–7 (log K_3, log K_2) and deprotonation of phosphonic groups is completed at pH above 8.2. The observed changes for the chemical shifts of pyridyl protons suggested that deprotonation of pyridine nitrogen occurs between pH 5 and 6, thus the pK_3 value was assigned to pyridine nitrogen. This conclusion is confirmed by the observed changes in the UV-vis spectra of the NP_2py ligand. The spectrophotometric titration curve is shown in Fig. 10.

As was mentioned above, the $^1\pi \rightarrow {}^1\pi^*$ and $^1n \rightarrow {}^1\pi^*$ band observed in the UV spectrum of the NP_2py ligand is particularly sensitive to the protonation of pyridine *N* (Fig. 3S†). A remarkable decrease of the ε value is observed between pH 5 and 7. This unequivocally confirms the attribution of log K_3 to the protonation of the pyridine moiety.

The minimalization of the sum equal to $\sum(\varepsilon_{exp} - \varepsilon_{calc})^2$ by using eqn (4) enabled us to determine the β_n values which are converted into K_n values (Table 5).

$$\varepsilon_{calc} = \frac{\varepsilon_L + [H]\beta_1\varepsilon_{HL} + [H]^2\beta_2\varepsilon_{H_2L} + [H]^3\beta_3\varepsilon_{H_3L} + [H]^4\beta_4\varepsilon_{H_4L}}{1 + [H]\beta_1 + [H]^2\beta_2 + [H]^3\beta_3 + [H]^4\beta_4} \quad (4)$$

where:

ε_{exp}, ε_{calc} – experimental and calculated absorption molar coefficients (M^{-1} cm^{-1}) at λ = 259.6 nm;

ε_L–ε_{H_nL} – absorption molar coefficients of individual species;

β_n – cumulative protonation constant.

Table 4 The protonation constants of H_4NP_2py in 25 °C in different ionic strengths and background electrolytes

	I [M]	log K_1 (HL)	log K_2 (H_2L)	log K_3 (H_3L)	log K_4 (H_4L)
0.1	$NaClO_4$	10.63(2)	6.74(6)	5.61(8)	2.23(9)
0.075	KCl	10.87(1)	6.55(2)	5.47(2)	2.17(2)
0.1	KCl	10.83(1)	6.61(2)	5.29(2)	1.60(6)
0.2	KCl	10.78(1)	6.41(2)	5.37(2)	2.00(3)
0.5	KCl	10.59(1)	6.27(2)	5.25(2)	1.60(6)
1	KCl	10.50(1)	6.17(2)	5.26(2)	2.01(4)
2	KCl	10.51(1)	6.19(2)	5.27(2)	1.60(8)

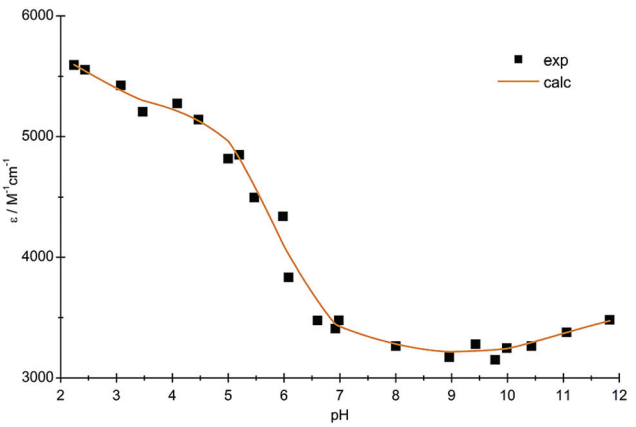

Fig. 10 Spectrophotometric titration curve of the NP_2py ligand.

Table 5 The comparison of the protonation constants of the NP_2py ligand using different methods

	^{31}P NMR[17]	UV-vis	Potentiometry
$\log K$ (HL)	10.9(9)	11.0(9)	10.63(2)
$\log K_2$ (H_2L)	6.7(9)	6.6(9)	6.74(6)
$\log K_3$ (H_3L)	5.5(9)	5.6(9)	5.61(8)
$\log K_4$ (H_4L)	2.3(9)	2.7(9)	2.23(9)
$\log K_5$ (H_5L)	0.98(5)	—	—
$\log K_6$ (H_6L)	0.70(5)	—	—

As is seen from Table 5 the values of the respective $\log K_n$ determined from different methods are the same, within the experimental error. Finally the calculated values of $\log K_n$ were used to determine the speciation distribution curve, which is presented in Fig. 6S.†

Formation constants. Potentiometric titrations of the Ln–NP_2py system (where Ln = Sm^{3+}, Eu^{3+}, Gd^{3+} and Tb^{3+}) were performed in order to determine the stoichiometry and stability constants of the formed complexes. The potentiometric measurements were performed for two Ln : NP_2py molar ratios 1 : 1 and 1 : 2. The calculated stability constants of LnL = $[Ln(NP_2py)]^-$ and LnL_2 = $[Ln(NP_2py)_2]^{5-}$ complexes (at 25 °C, I_{NaClO_4} = 0.1 M) are collected in Table 3S† and selected values are shown in Table 6.

The species distribution curves are depicted in Fig. 7S.† The potentiometric measurements of Eu : NP_2py = 1 : 1 and 1 : 2 systems at different ionic strengths (KCl) were also performed and the determined stability constants are given in Table 4S.†

Based on potentiometric data it was possible to calculate $\log K_{12}$ for reaction 2, which is equal to 5.27 and similar within the limit of experimental error to that estimated from the spectroscopic data (4.4 ± 0.5).

The determined stability constants for Eu–NP_2py systems were used to calculate the average ligand number (ñ) as a function of pH (Fig. 11). The data for the Eu–NTA (1 : 2) complex (where NTA is nitrilotriacetic acid) are also included in this figure for comparison purposes.[29a]

As is seen in Fig. 11 the coordination of the NP_2py ligand to the Eu^{3+} starts at about pH 3 for 1 : 1 and 1 : 2 complexes. In the case of the Eu : NP_2py 1 : 2 system the formation of the $[Ln(NP_2py)_2]^{5-}$ complex starts at about pH 8 and it is consistent with the spectroscopic data described above. The difference between Eu–NTA and Eu–NP_2py complexes with the molar ratio 1 : 2 is clearly seen. The coordination of two NTA ligands occurs at low pH ~ 2[29] and is completed at pH ~ 6. As far as Eu–NP_2py of the 1 : 2 system is concerned, the $[Eu(NP_2py)]^-$ complex is a predominating species within the pH range 3–9 and the formation of the $[Eu(NP_2py)_2]^{5-}$ complex takes place at pH above 8. This may be explained qualitatively by considering the formal charge of reacting species. In the case of the Ln–NTA system the neutral LnNTA complex reacts with the H_nNTA ligand to form finally $[Ln(NTA)_2]^{3-}$ species with the formal charge −3. The formal charge of the $Ln(NP_2py)_2$ complex is −5 and the formed complex is not as stable as $[Ln(NTA)_2]^{3-}$. Out of the considered complexes, the $[Ln(NTP)_2]^{9-}$ one is the most negatively charged, therefore this may suggest that the stability of the complexes should change in the following order: $Ln(NTA)_2$ > $Ln(NP_2py)_2$ > $Ln(NTP)_2$. Such an assumption is consistent with potentiometric results derived from Sawada *et al.*[14] These authors have shown that only the $[Ln(NTP)]^{3-}$ complex is formed in solution, on the other hand Kozlovski *et al.*[16] assumed the existence of both – $[Ln(NTP)]^{3-}$ and $[Ln(NTP)_2]^{9-}$ species.

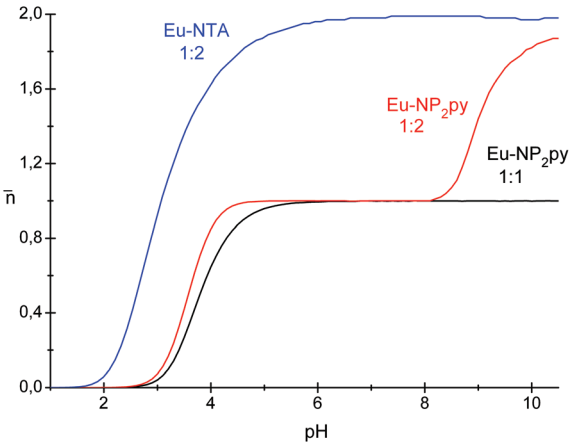

Fig. 11 The average ligand number ñ as a function of pH for Eu–NTA (1 : 2 ratio) as well as for Eu–NP_2py complexes (1 : 2 and 1 : 1 ratios).

Table 6 The stability constants of Ln^{3+} complexes with the NP_2py ligand for Ln : NP_2py molar ratios of 1 : 1 and 1 : 2, at 25 °C, I = 0.1 mol dm^{-1} ($NaClO_4$)

Ln : NP_2py	1 : 1 $\log \beta_{LnL}$	1 : 2 $\log \beta_{LnL}$	$\log \beta_{LnL_2}$
Sm^{3+}	11.87(6)	11.83(5)	16.99(8)
Eu^{3+}	12.85(8)	12.85(6)	18.44(9)
Gd^{3+}	12.32(10)	12.45(6)	17.88(7)
Tb^{3+}	13.36(7)	13.47(10)	17.86(9)

Extrapolation of $[Eu(NP_2py)]^-$ and $[Eu(NP_2py)_2]^{5-}$ stability constants to zero ionic strength

The SIT approach (Specific Ion Interaction Theory)[18] was used for the extrapolation and correction of equilibrium data to the infinite dilution standard state. This simple method provides good estimations of activity coefficients and is recommended for use by the OECD Nuclear Energy Agency.[30] The extrapolation of the formation constants to ionic strength equal to zero requires the estimation of activity coefficients of all species that participated in chemical reactions. This may be performed by the SIT model. For the reactions:

$$L^{4-} + nH^+ \rightleftarrows H_nL^{-4+n} \quad (5)$$

$$Eu^{3+} + mL^{5-} \rightleftarrows [EuL_m]^{-4m+3}. \quad (6)$$

According to the SIT procedure, the logarithms of stability constants at a fixed ionic strength $\log \beta_n(\mathrm{I})$ are related to the corresponding logarithms of thermodynamic constants β_n^0 by the following equations:

$$\log \beta^0_{\mathrm{H}_n\mathrm{L}} = \log \beta_{\mathrm{H}_n\mathrm{L}}(I_m) + \log \gamma_{H_nL} - \log \gamma_L - n \log \gamma_H \quad (7)$$

$$\log \beta^0_{\mathrm{EuL}_m} = \log \beta_{\mathrm{EuL}_m}(I_m) + \log \gamma_{\mathrm{EuL}_m} - \log \gamma_{\mathrm{Eu}} - m \log \gamma_{\mathrm{L}} \quad (8)$$

where γ are activity coefficients of individual species.

The $\log \gamma_j$ of the j-species may be calculated by using the following formula:

$$\log \gamma_j = -z_j^2 \frac{0.509\sqrt{I_m}}{1 + 1.5\sqrt{I_m}} + \varepsilon_j I_m \quad (9)$$

where:

z – charge of the j-species;

I_m – ionic strength of solution expressed in mol kg^{-1};

ε_j – the interaction coefficient of ion pairs.

Combining eqn (8) or (9) with (10), the following equations are derived:

$$\log \beta_{\mathrm{H}_n\mathrm{L}}(I_m) + \Delta z^2 \frac{0.509\sqrt{I_m}}{1 + 1.5\sqrt{I_m}} = \log \beta^0_{\mathrm{H}_n\mathrm{L}} - \Delta\varepsilon_{\mathrm{H}_n\mathrm{L}} I_m \quad (10)$$

$$\log \beta_{EuL_m}(I_m) + \Delta z^2 \frac{0.509\sqrt{I_m}}{1 + 1.5\sqrt{I_m}} = \log_{10} \beta^0_{EuL_m} - \Delta\varepsilon_{EuL_m} I_m \quad (11)$$

where:

$\Delta z^2 = \sum z^2_{\mathrm{products}} - \sum z^2_{\mathrm{substrates}}$;

$\Delta\varepsilon^2 = \sum \varepsilon^2_{\mathrm{products}} - \sum \varepsilon^2_{\mathrm{substrates}}$.

Linear regressions of eqn (10) and (11), using the experimental values of $\log \beta(I_m)$ and I_m give the thermodynamic values of $\log \beta^0_{\mathrm{H}_n\mathrm{L}}$ and $\log \beta^0_{\mathrm{EuL}_m}$ (Table 7).

In general, these data may be useful in finding a reliable, thermodynamic model of the complexation reaction of aminophosphonic ligands with lanthanides particularly that, to the best of our knowledge, there are no stability constants of lanthanide/actinide phosphonates extrapolated to the zero ionic strength. This is the reason for which we are unable to refer our data to other ones.

Table 7 Formation constants $\log \beta^0_{\mathrm{AB}}$ of compounds under study at the zero ionic strength at 25 °C

AB	$\log \beta^0_{\mathrm{AB}}$	$\Delta\varepsilon$	R^2
HL	11.8 ± 0.05	−0.31 ± 0.05	0.92
H_2L	19.0 ± 0.05	−0.48 ± 0.04	0.98
H_3L	24.6 ± 0.11	−0.88 ± 0.10	0.96
H_4L	26.9 ± 0.26	−0.76 ± 0.25	0.76
EuL	16.3 ± 0.11	−0.82 ± 0.11	0.95
EuL_2	19.5 ± 0.15	−0.46 ± 0.15	0.77

Summary and conclusions

The compounds of the formula $[C(NH_2)_3]_5[Ln(NP_2py)_2]\cdot 12H_2O$ (where Ln = Eu, Gd) with new tripodal NP_2py ligands were synthesized and their crystal structure was determined. The crystal comprises monomeric $[Eu(NP_2py)_2]^{5-}$ anions. Both ligands are bonded with the Eu^{3+} cation by two oxygen atoms from monodentate phosphonic groups, one tertiary nitrogen atom and one pyridine nitrogen atom, filling thus the eight coordination sites of the Eu^{3+} cation. The approximate C_i symmetry of the $[Eu(NP_2py)_2]^{5-}$ complex is reflected in the luminescence spectra, in which the intensity of the magnetic dipole $^5D_0 \rightarrow {}^7F_1$ transition dominates over the intensities of the remaining $^5D_0 \rightarrow {}^7F_{0,2,3,4}$ transitions.

The luminescence spectra of Eu–NP_2py and Tb–NP_2py complexes in aqueous solutions at different pH with various Ln : L ratios were studied in order to find the coordination mode of the NP_2py ligand and the stoichiometry of complexes. The NP_2py ligand starts to coordinate through phosphonic oxygen atoms with Ln^{3+} at pH ~ 2. The coordination of the pyridyl group to the Tb^{3+} occurs at pH between 3.0 and 5.5. The binding of the NP_2py ligand is completed above pH = 6.

This study has demonstrated that both $[Ln(NP_2py)]^-$ and $[Ln(NP_2py)_2]^{5-}$ complexes exist in solution, however, the $[Ln(NP_2py)_2]^{5-}$ starts to form at pH as high as 8. The comparison of the luminescence spectra of the $[C(NH_2)_3]_5[Eu(NP_2py)_2]\cdot 12H_2O$ crystals with those of Eu : NP_2py (1 : 2) solutions enabled us to estimate the molar fraction of $[Eu(NP_2py)]^-$ (~19%) and $[Eu(NP_2py)_2]^{5-}$ (~81%) complexes at pH = 10.5, and finally, to calculate the conditional formation constant of reaction $[Eu(NP_2py)]^- + NP_2py^{4-} \rightleftarrows [Eu(NP_2py)_2]^{5-}$ ($\log K_{12}$ = 4.4 ± 0.5).

The potentiometric measurements were applied to determine the stability constants of complexes under study. The stability constants are between 11.83(5) for $[Sm(NP_2py)]^-$ and 13.47(7) for $[Tb(NP_2py)]^-$ and are slightly lower than those obtained for Ln–NTP complexes.[16] Thus, the substitution of one phosphonic group by a pyridyl moiety slightly affects the stability of the $[Ln(NP_2py)]^-$ complex in comparison with the $[Ln(NTP)]^{3-}$ one.[16] On the other hand the $\log \beta^0_{LnL_2}$ of the $[Ln(NP_2py)_2]^{5-}$ complexes are about 5–6 orders smaller in comparison with those reported for $[Ln(NTP)_2]^{9-}$.[16] It should be noted, however, that the existence of $[Ln(NTP)_2]$ complexes in solution has not been proved unequivocally.[14–16]

Potentiometric titrations at various ionic strengths were also performed in order to find the thermodynamic stability constants of $[Eu(NP_2py)]^-$ and $[Eu(NP_2py)_2]^{5-}$ complexes. Such data are, in principle, preferable as a basis for discussion on the factors governing the stabilities of the complexes. The extrapolation of the formation constants to zero ionic strength under standard conditions was performed by the SIT procedure. The estimated $\log \beta^0_{\mathrm{EuL}}$ and $\log \beta^0_{\mathrm{EuL}_2}$ values are 16.3 ± 0.11 and 19.5 ± 0.15, respectively. For lanthanide aminophosphonate complexes there are no thermodynamic quantities in the literature therefore we refer the obtained data to the well-known $[Eu(NTA)]$ and $[Eu(NTA)_2]^{3-}$ complexes, only.[29] The

latter are characterized by the thermodynamic stability constants: $\log \beta^0_{EuNTA} = 13.34$ and $\log \beta^0_{Eu(NTA)_2} = 22.66$.

Taking into account all these data one may conclude that the high negative charge of a ligand may stabilize the LnL complex, but simultaneously destabilizes the LnL_2 one.

Experimental

Materials

All chemicals used were of analytical grade. The stock solutions of anhydrous Ln^{3+} chlorides (Aldrich) were standardized against EDTA using xylenol orange as an indicator. *N*-(methylene-2-pyridine)-*N*,*N*-di(methylenephosphonate) as a diammonium dihydrogen compound was synthesized as described previously.[17]

Crystal preparation

The crystals of the formula $[C(NH_2)_3]_5[Ln(NP_2py)_2]\cdot 12H_2O$ (Ln = Eu or Gd) were obtained in the following way:

The suspension of 0.5 mmol Ln_2O_3 (Eu_2O_3 Stanford Materials 99.995%, Gd_2O_3 Stanford Materials 99.99%) and of 2.2 mmol $(NH_4)_2H_2NP_2py$ salt in H_2O were heated at 90 °C ± 5 °C. After dissolution of the reagents, the solution was alkalized by using $[C(NH_2)_3]_2CO_3$ to the final pH ~ 10.5 and left for crystallization. The colourless crystals were formed after three months.

The luminescence quantum yields for solutions of the Tb^{3+}-NP_2py complexes were determined in relation to fluorescein in 0.1 M NaOH (Φ = 93%), by using eqn (13):

$$Q_X = Q_S \cdot \frac{n_X^2}{n_S^2} \cdot \frac{\int_{\bar{\nu}_1}^{\bar{\nu}_2} I_X(\bar{\nu})\mathrm{d}\bar{\nu}}{\int_{\bar{\nu}_1}^{\bar{\nu}_2} A_S(\bar{\nu})\mathrm{d}\bar{\nu}} \cdot \frac{1-10^{-\varepsilon_S \cdot d \cdot c_S}}{1-10^{-\varepsilon_X \cdot d \cdot c_X}} \quad (13)$$

where Q stands for the quantum yield, n is the refraction index (n_X = 1.38, n_S = 1.33), the integrals were taken for the emission spectra corrected for the instrument response, ε is the molar absorption coefficient, c – concentration, and d – thickness of the cuvette (1 cm). The subscripts X and S stand for the sample and the standard, respectively. The pairs of the sample and the standard spectra used in the above equation were taken at the same instrument setting (slit widths, photomultiplier voltage *etc.*). The slits were 1 nm for the excitation and 1 nm for the emission recording.

Elemental analysis. $C_{21}H_{74}EuN_{19}O_{24}P_4$: $N\%_{calc}$ – 21.24%, $N\%_{exp}$ – 20.85%, $C\%_{calc}$ – 20.13%, $C\%_{exp}$ – 20.56%, $H\%_{calc}$ – 5.95%, $H\%_{exp}$ – 5.28%; $C_{21}H_{74}GdN_{19}O_{24}P_4$: $N\%_{calc}$ – 21.15%, $N\%_{exp}$ – 22.48%, $C\%_{calc}$ – 20.05%, $C\%_{exp}$ – 21.56%, $H\%_{calc}$ – 5.93%, $H\%_{exp}$ – 5.30%.

X-Ray crystal analysis

The crystallographic measurements were performed on an Xcalibur, Sapphire2 four-circle diffractometer with graphite-monochromatized MoKα radiation. The data for the crystal were collected at 100(2) K using the Oxford Cryosystems cooler and were analytically corrected for absorption with the use of the CrysAlis RED program of the Xcalibur software. The structures were solved routinely by using Patterson synthesis. The C- and N-bonded hydrogen atoms were placed in positions calculated from the geometry. The final refinement was anisotropic for all non-H atoms. The computations were performed with the SHELXS97[31] and SHELXL97 programs,[32] and the molecular graphics was prepared with XP–Interactive Molecular Graphics.[33] High residual peaks suggest that the C50 guanidine cation is partially distorted, however it was not possible to resolve this distortion. A summary of the conditions for the data collection and the structure refinement parameters is given in Table 8.

Table 8 Crystal data

CCDC no.	CCDC 1541895	CCDC 1541894
Chemical formula	$C_{21}H_{74}EuN_{19}O_{24}P_4$	$C_{21}H_{74}GdN_{19}O_{24}P_4$
M_r	1252.83	1258.12
Crystal system, space group	Triclinic, $P\bar{1}$	Triclinic, $P\bar{1}$
Temperature (K)	100(2)	100(2)
a, b, c (Å)	11.9255 (11), 14.1373 (12), 16.1417 (15)	11.9496 (6), 14.1528 (7), 16.1651 (9)
α, β, γ (°)	105.889 (8), 94.515 (7), 90.629 (7)	105.710 (5), 94.360 (4), 90.901 (4)
V (Å^3)	2607.8 (4)	2622.2 (2)
Z	2	2
μ (mm^{-1})	1.39	1.48
Crystal size (mm)	0.45 × 0.07 × 0.04	0.27 × 0.05 × 0.02
T_{min}, T_{max}	0.709, 0.958	0.816, 0.979
No. of measured, independent and observed [$I > 2\sigma(I)$] reflections	51 538, 25 885, 19 822	23 976, 15 463, 8529
R_{int}	0.053	0.093
$(\sin\theta/\lambda)_{max}$ (Å^{-1})	0.851	0.737
$R[F^2 > 2\sigma(F^2)]$, w$R(F^2)$, S	0.061, 0.147, 1.15	0.101, 0.184, 1.05
No. of reflections	25 885	15 463
No. of parameters	601	601
No. of restraints	6	6
$\Delta\rho_{max}$,$\Delta\rho_{min}$(e Å^{-3})	4.71, −2.10	1.26, −1.25

Spectroscopic measurements

Luminescence spectra and luminescence lifetimes were recorded on an Edinburgh Instruments FLS 920 spectrometer at RT. UV-vis absorption spectra were recorded on a Cary 500 UV/Vis/NIR spectrophotometer.

Potentiometric titrations

The solution studies were carried out in double-distilled water. The titrations were performed using a MOLSPIN pH-meter system equipped with a Mettler Toledo InLab® Micro electrode filled with 3 M KCl and the automatic burette. The electrode was calibrated daily against hydrogen concentrations using $HClO_4$ (Merck) or HCl (POCh) according to the procedure of Irving *et al.*[34] The purity and exact concentration of the ligand were determined by the method of Gran.[35] Alkali, carbonate-free, was standardized by titration with potassium hydrogen phthalate (Merck).

Measurements in 0.1 M ionic strength:

The ionic strength was fixed at I = 0.1 M with $NaClO_4$ (VWr). The ionic product of water under the used conditions was $10^{-13,77}$ mol^2 dm^{-6}. Alkali: 0.1 M sodium hydroxide solution (Aldrich).

Measurements in various ionic strengths:

The ionic strength was fixed at I = 0.075 M, 0.1 M, 0.2 M, 0.5 M, 1 M and 2 M with KCl (POCh). The ionic product of water under the used conditions was $10^{-13,78}$, $10^{-13,77}$, $10^{-13,72}$, and $10^{-13,75}$ mol^2 dm^{-6}, respectively.[36] Alkali: 0.1 M potassium hydroxide solution (Aldrich).

All the titrations were carried out on 2.0–3.0 ml samples at 25 ± 0.2 °C under an atmosphere of Ar. SUPERQUAD[37] and HYPERQUAD2008[38] computer programs that use non-linear least-squares methods[39] were applied to calculate the stability constants. The results were obtained in the form of concentration overall stability constants $\beta_{pqr} = [M_pH_qL_r]/[M]^p[H]^q[L]^r$, where M stands for metal, H is proton and L the deprotonated form of the ligand. They are, however, a good indication of the importance of a particular species in the equilibrium. Triplicate titrations of the free ligand (number of recorded points: 150–180) and the complexes were carried out at metal to ligand ratios 1 : 1 and 1 : 2 (number of recorded points: 180–210). Each time about 120–150 and 150–190 titration points have been used for the calculations, respectively. The ligand concentration was 0.7–1 × 10^{-3} mol dm^{-3} in all titrations. No precipitation was noticed in any titration. The distribution curve of the protonated species of L as a function of pH was calculated using the HySS2009 program.[40]

The ligand used for potentiometric measurements was in the form of a diammonium salt ($(NH_4)_2H_2NP_2py$); NP_2py = $[H_6L]^{2+}$ in order to improve its solubility in water. Therefore two ammonium cations were also considered in the overall acid–base equilibrium calculations of the compound. The determined values of the protonation constants which belong to the ammonia $\log K_{NH4}$ vary within the range 8.98(1)–9.73(1) for different studied ionic strengths and are very close to those previously reported in the literature: $\log K$ = 9.38(1),[41] $\log K$ = 9.50,[42] $\log K$ = 9.10(3),[43] (I = 0.1 M).

CAUTION! Although no problems were encountered in this work, transition metal perchlorate complexes are potentially explosive and should be handled with appropriate precautions.

Acknowledgements

This work was supported by MNiSW grant no 2273/M/WCH/12.

References

1 (*a*) W. A. Volkert and T. J. Hoffmann, *Chem. Rev.*, 1999, **99**, 2269–2292; (*b*) E. Gumienna-Kontecka and J. Gałęzowska, *Coord. Chem. Rev.*, 2012, **256**, 105–124; (*c*) J. Goura and V. Chandrasekhar, *Chem. Rev.*, 2015, **115**, 6854–6965; (*d*) J. A. Amoroso, I. A. Fallis and S. J. A. Pope, *Coord. Chem. Rev.*, 2017, **340**, 198–219; (*e*) A. D. G. Firmino, R. F. Mendes, M. M. Antunes, P. C. Barbosa, S. M. F. Vilela, A. A. Valente, F. M. L. Figueiredo, J. P. C. Tome and F. A. A. Paz, *Inorg. Chem.*, 2017, **56**, 1193–1208.

2 L. Lukeš, J. Kotek, P. Vojtisek and P. Hermann, *Coord. Chem. Rev.*, 2001, **216–217**, 287.

3 (*a*) R. Janicki and P. Starynowicz, *Acta Crystallogr., Sect. B: Struct. Sci.*, 2010, **66**, 559–567; (*b*) R. Janicki, A. Kędziorki and A. Mondry, *Phys. Chem. Chem. Phys.*, 2016, **18**, 27808–27817.

4 A. Mermer and P. Starynowicz, *Acta Crystallogr., Sect. B: Struct. Sci.*, 2011, **67**, 399–408.

5 (*a*) T. Kiss, J. Balla, G. Nagy, H. Kozlowski and T. Jankowska, *Inorg. Chim. Acta*, 1987, **138**, 25–30; (*b*) T. Kiss and I. Lazar, in *Aminophosphonic and Aminophosphinic Acids: Chemistry and Biological Activity*, ed. P. V. Kukhar and H. R. Hudson, Wiley, NY, 2000, pp. 285–325.

6 (*a*) G. Ch. de Witt, P. M. May, J. Webb and G. Hefter, *BioMetals*, 1996, **9**, 351–361; (*b*) A. D. Sherry, J. Ren, J. Huskens, E. Brücher, E. Tóth, C. F. C. G. Geraldes, M. M. C. A. Castro and W. P. Cacheris, *Inorg. Chem.*, 1996, **35**, 4604–4612; (*c*) J. E. Bollinger and D. M. Roundhill, *Inorg. Chem.*, 1993, **32**, 2821–2826; (*d*) J. Gałęzowska, R. Janicki, A. Mondry, R. Burgada, T. Bailly, M. Lecouvey and H. Kozlowski, *Dalton Trans.*, 2006, 4384–4394; (*e*) A. Mondry and R. Janicki, *Dalton Trans.*, 2006, 4702–4710; (*f*) R. Janicki and A. Mondry, *Polyhedron*, 2008, **27**, 1942–1946; (*g*) R. Janicki and A. Mondry, *Eur. J. Inorg. Chem.*, 2013, 3429–3438; (*h*) R. Janicki, M. Monteil, M. Lecouvey and A. Mondry, *Opt. Mater.*, 2013, **36**, 259–264; (*i*) J. Gałęzowska, R. Janicki, H. Kozłowski, A. Mondry, P. Młynarz and Ł. Szyrwiel, *Eur. J. Inorg. Chem.*, 2010, 1696–1702.

7 (*a*) J. C. G. Bünzli and C. Piguet, *Chem. Soc. Rev.*, 2005, **4**, 1048–1077; (*b*) J. C. G. Bünzli and S. V. Eliseeva, *Chem. Sci.*, 2013, **4**, 1939–1949.
8 J.-G. Mao, *Coord. Chem. Rev.*, 2007, **251**, 1493–1520.
9 (*a*) A. L. Tiwari, H. Ojha, A. Kaul, A. Dutta, P. Srivastava, G. Shukla, R. Srivastava and A. K. Mishra, *Chem. Biol. Drug Des.*, 2009, **7**, 87–91; (*b*) É. Tóth, L. Helm and A. E. Merbach, in *The Chemistry of Contrast Agents in Medical Magnetic Resonance Imaging*, ed. A. E. Merbach, L. Helm and É. Tóth, Wiley, Chichester, UK, 2nd edn, 2013, pp. 25–76; (*c*) S. Marinim, Y. Huang, D. Coman and F. Hyder, *J. Biol. Inorg. Chem.*, 2014, **19**, 1385–1398; (*d*) M. Elhabiri, S. Abada, M. Sy, A. Nonat, P. Choquet, D. Esteban-Gómez, C. Cassino, C. Platas-Iglesias, M. Botta and L. J. Charbonnière, *Chem. – Eur. J.*, 2015, **21**, 6535–6546.
10 A. D. Sherry and C. F. G. C. Geraldes, in *Lanthanide Probes in Life, Chemical and Earth Sciences, Theory and Practice*, ed. J. C. Bünzli and G. Choppin, Elsevier, Amsterdam, 1989, p. 93.
11 US FDA Approval for Quadramet, 28/09/97 (NDA) 020570.
12 (*a*) H. Studnik, S. Liebsch, G. Forlani, D. Wieczorek, P. Kafarski and J. Lipok, *New Biotechnol.*, 2015, **32**(1), 1–6; (*b*) B. Nowack, *Water Res.*, 2002, **36**, 4636–4642.
13 (*a*) P. Silva, F. Vieira, A. C. Gomes, D. Ananias, J. A. Fernandes, S. M. Bruno, R. Soares, A. A. Valente, J. Rocha and F. A. Almeida Paz, *J. Am. Chem. Soc.*, 2011, **133**, 15120–15138; (*b*) R. F. Mendes, P. Silva, M. M. Antunes, A. A. Valente and F. A. Almeida Paz, *Chem. Commun.*, 2015, **51**, 10807–10810.
14 K. Sawada, M. Kuribayashi, T. Suzuki and H. Miyamoto, *J. Solution Chem.*, 1991, **20**, 829–839.
15 R. C. Holz, G. E. Meister and W. Dew. Horrocks Jr., *Inorg. Chem.*, 1990, **29**, 5183–5189.
16 E. Kozlovski, S. Aleksandrov and L. Chesnokova, *Zh. Neorg. Khim.*, 2002, **47**, 1566–1568.
17 R. Janicki, *J. Mol. Struct.*, 2013, **1036**, 35–41.
18 (*a*) J. N. Brønsted, *J. Am. Chem. Soc.*, 1922, **44**, 877–898; (*b*) J. N. Brønsted, *J. Am. Chem. Soc.*, 1922, **44**, 938–948; (*c*) E. A. Guggenheim, *Philos. Mag.*, 1935, **19**, 588–643; (*d*) G. Scatchard, *Chem. Rev.*, 1936, **19**, 309–327.
19 R. S. Dickins, D. Parker, J. I. Bruce and D. J. Tozer, *Dalton Trans.*, 2003, 1264–1271.
20 (*a*) M. Pan, X. L. Zheng, Y. Liu, W. S. Liu and C. Y. Su, *Dalton Trans.*, 2009, 2157–2169; (*b*) Q. Y. Yang, K. Wu, J. J. Jiang, C. W. Hsu, M. Pan, J. M. Lehn and C. Y. Su, *Chem. Commun.*, 2014, **50**, 7702–7704; (*c*) B. B. Du, a Y. X. Zhu, M. Pan, M. Q. Yue, Y. J. Hou, K. Wu, L. Yin Zhang, L. Chen, S. Y. Yin, Y. N. Fana and C. Y. Su, *Chem. Commun.*, 2015, **51**, 12533–12536; (*d*) E. Kasprzycka, V. A. Trush, V. M. Amirkhanov, L. Jerzykiewicz, O. Malta, J. Legendziewicz and P. Gawryszewska, *Chem. – Eur. J.*, 2017, **23**, 1318–1330.
21 (*a*) C. Görller-Walrand, C. L. Fluyt, A. Ceulemans and W. T. Carnall, *J. Chem. Phys.*, 1991, **95**, 3099; (*b*) C. Görller-Walrand and K. Binnemans, in *Handbook on the Physics and Chemistry of Rare Earths Vol. 25*, ed. K. A. Gschneidner and L. Eyring, Elsevier, 1998, vol. 167, pp. 121–125.
22 (*a*) M. Latva, H. Takalo, V. M. Mukkala, C. Matachescu, J. C. Rodriguez-Ubis and J. Kankare, *J. Lumin.*, 1995, **75**, 149–169; (*b*) L. Smętek and A. Kędziorski, *J. Lumin.*, 2010, **130**, 1154–1159.
23 (*a*) R. Janicki and A. Mondry, *Phys. Chem. Chem. Phys.*, 2015, **16**, 26823–26831; (*b*) R. Janicki and A. Mondry, *Phys. Chem. Chem. Phys.*, 2015, **17**, 29558–29565.
24 K. Bukietyńska, A. Mondry, P. N. Thuy and P. Starynowicz, *J. Alloys Compd.*, 1995, **225**, 52–54.
25 C. K. Sawada, T. Araki and T. Suzuki, *Inorg. Chem.*, 1987, **26**, 1199.
26 G. Grossmann, K. A. Burkov, G. Hägele, L. A. Myund, S. Hermens, C. Verwey and S. M. Arat-ool, *Inorg. Chim. Acta*, 2004, **357**, 797.
27 V. Deluchat, J.-C. Bolliner, B. Shepaud and C. Caullet, *Talanta*, 1997, **44**, 897.
28 B. Kurzak, A. Kamecka, K. Kurzak, J. Jezierska and P. Kafarski, *Polyhedron*, 2000, **19**, 2083.
29 (*a*) G. Anderegg, *Pure Appl. Chem.*, 1982, **54**, 2693–2758; (*b*) K. Bukietyńska and A. Mondry, *Inorg. Chim. Acta*, 1987, **130**, 271–276.
30 I. Grenthe, F. Mompean, K. Spahiu and H. Wanner, *Guidelines for the extrapolation to zero ionic strength*, OECD Nuclear Energy Agency, Data Bank, 2013.
31 G. M. Sheldrick, *SHELXS-97, program for structure solution*, University of Göttingen, 1997.
32 G. M. Sheldrick, *SHELXL-97, program for structure refinement*, University of Göttingen, 1997.
33 40 XP–Interactive Molecular Graphics, v. 5.1–Bruker Analytical X-ray Systems 1998.
34 H. M. Irving, M. G. Miles and L. D. Pettit, *Anal. Chim. Acta*, 1967, **38**, 475–488.
35 G. Gran, *Acta Chem. Scand.*, 1950, **4**, 559–577; G. Gran, *Analyst*, 1952, **77**, 661–671.
36 F. H. Sweeton, R. E. Mesmer and C. F. Baes Jr., *J. Solution Chem.*, 1974, **3**(3), 191–214.
37 P. Gans, A. Sabatini and A. Vacca, *J. Chem. Soc., Dalton Trans.*, 1985, 1195–1200.
38 P. Gans, A. Sabatini and A. Vacca, *Talanta*, 1996, **43**, 1739–1753.
39 P. Gans, *Data Fitting in the Chemical Sciences*, John Wiley & Sons, Chichester, 1992.
40 L. Alderighi, P. Gans, A. Ienco, D. Peters, A. Sabatini and A. Vacca, *Coord. Chem. Rev.*, 1999, **184**, 311–318.
41 N. Saha and H. Sigel, *J. Am. Chem. Soc.*, 1982, **104**, 4100.
42 S. Kim and R. Martin, *J. Am. Chem. Soc.*, 1984, **106**, 1707.
43 W. N. Perera and G. Senanayake, *Inorg. Chem.*, 2004, **43**, 3048.

